in Table 2. End-diastolic LV diameter and end-systolic LV diameter did not significantly differ among the four groups. LV systolic function was assessed using percent fractional shortening (%FS) and LV diastolic function was assessed using the E/A ratio and c-IRT. Using these measurements, the data show that the administration of angiotensin over a 28-day period did not cause any abnormalities in systolic performance. However, the E/A ratio was reduced and c-IRT was prolonged in the Sal/AII group, indicating that there was some evidence of diastolic dysfunction after angiotensin administration. Finally, the data show that pravastatin treatment did improve the diastolic dysfunction caused by administration of angiotensin II.

Effects on Cardiac Hypertrophy

LV weight/body weight (LVW/BW) is summarized in Table 1. Angiotensin II treatment could increase the LVW/BW in mice. This increase of LVW/BW was strongly inhibited by pravastatin treatment. LV hypertrophy judged by posterior wall thickness and myocyte cross-sectional area was also clearly induced by angiotensin II treatment, which was significantly attenuated by pravastatin administration (Fig. 1 and Table 2).

Effects on Cardiac Fibrosis

Representative photomicrographs of the heart and coronary arteries are shown in Figs. 2 and 3. There was a substantial difference in the amount of interstitial and perivascular fibrosis between Sal/AII and Pra/AII treated mice (Figs. 2A and 3A). A significant degree of cardiac fibrosis was observed among cardiomyocytes and the surrounding coronary arteries in Sal/AII but not in Pra/AII mice. Quantitative immunohistochemical analyses showed that an infusion of angiotensin II increased both interstitial and perivascular fibrosis to a greater extent in Sal/AII than in Pra/AII mice (Figs. 2B and 3B). This indicates that pravastatin could attenuate cardiac fibrosis in angiotensin II-induced hypertensive mice.

Effects on Gene Expression

Using RT-PCR and real time-PCR, we analyzed critical markers of fibrosis and cardiac hypertrophy such as TGF-β,

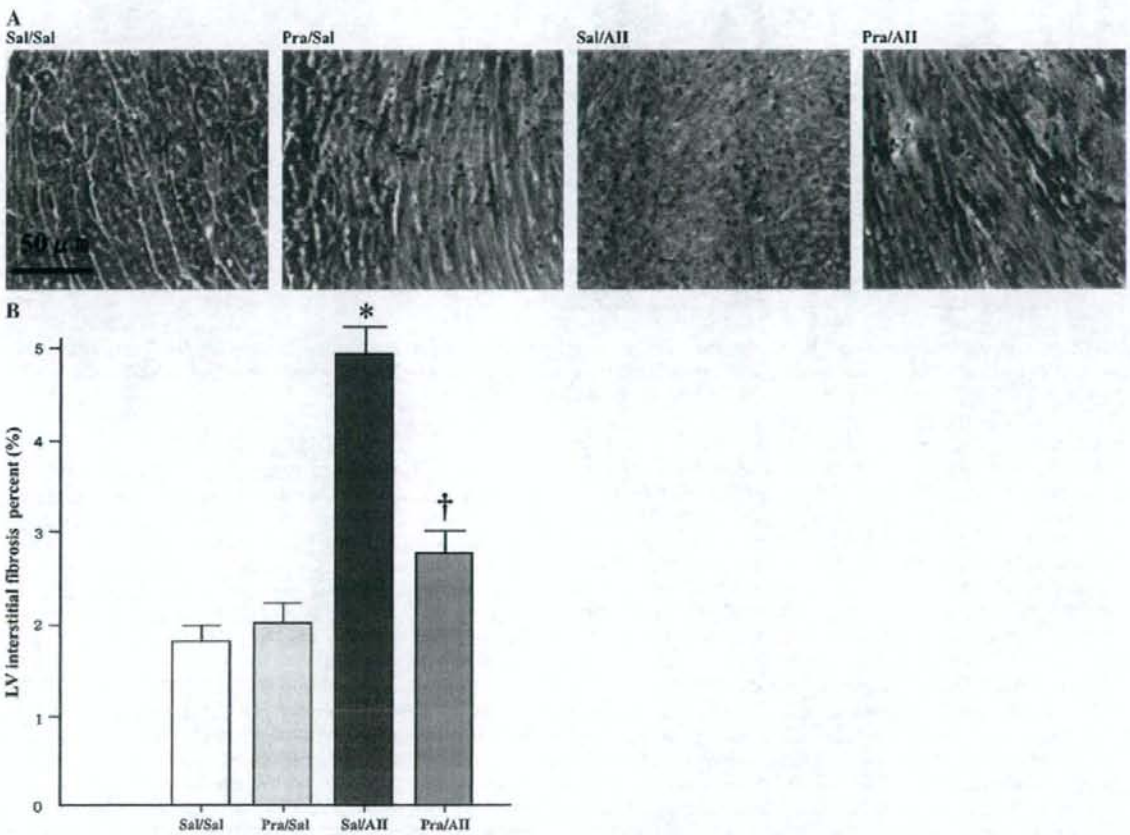

FIGURE 2. LV interstitial fibrosis in mice. A, Representative images of myocardium with intersririal fibrosis stained with Masson's trichrome stain. B, Bar graph shows quantified interstitial fibrotic area (%). Values are means ± SEM (Sal/Sal: n = 8, Pra/Sal: n = 9, Sal/AII: n = 15, Pra/AII: n = 16). *$P < 0.05$ vs. Sal/Sal and Pra/Sal; †$P < 0.05$ vs. Sal/AII.

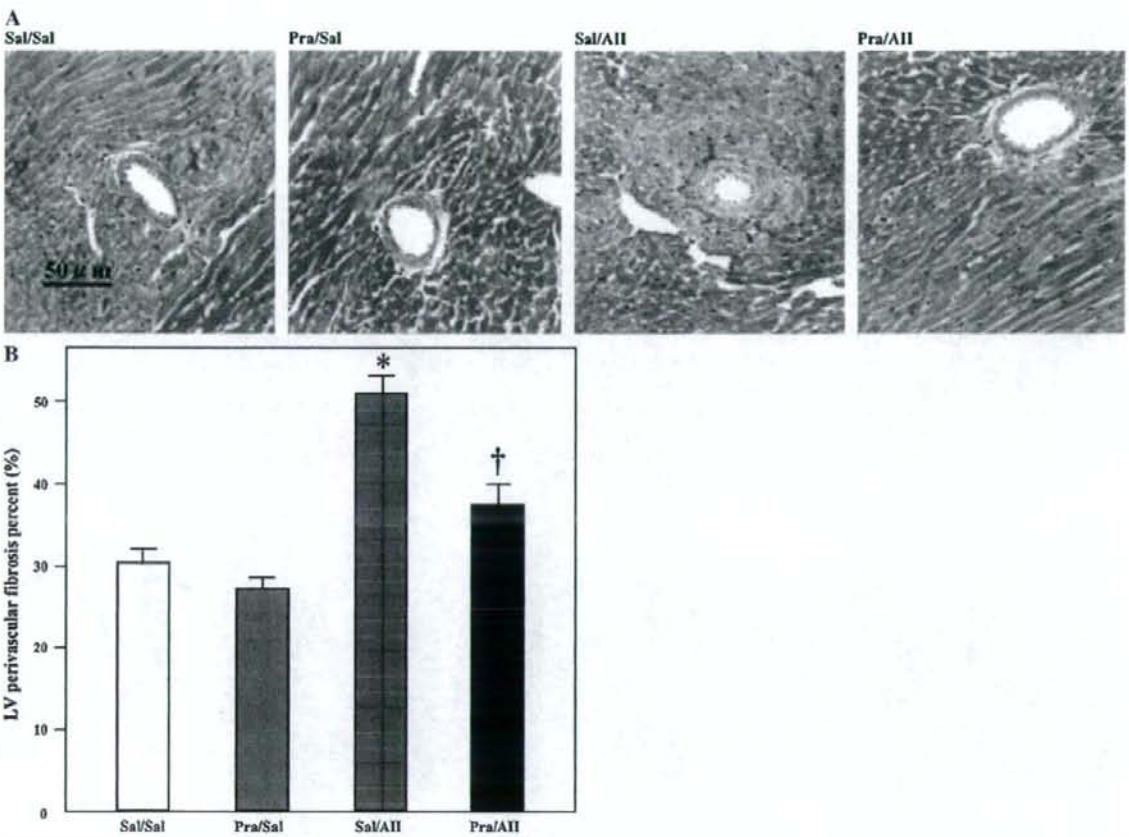

FIGURE 3. LV perivascular fibrosis in mice. A, Representative images of intramuscular arteries with perivascular fibrosis stained with Masson's trichrome stain. B, Bar graph shows quantified perivascular fibrotic areas (%). Values are means ± SEM (Sal/Sal: n = 8, Pra/Sal: n = 9, Sal/AII: n = 15, Pra/AII: n = 16). *$P < 0.05$ vs. Sal/Sal and Pra/Sal.

collagen I, ANF, ROCK1, IL-6, TNF-α, MMP-2 and -3, and the inverse regulator eNOS. An angiotensin II infusion increased TGF-β, ANF, IL-6, TNF-α, ROCK1, and collagen I mRNA expression. However, this increase was markedly less in Pra/AII mice. Interestingly, the expression of MMPs was enhanced by angiotensin II and the administration of pravastatin could inhibit this increase. Also, when compared to Sal/AII-treated mice, the expression of eNOS significantly increased in pravastatin-treated mice (Fig. 4A and B).

Effects on ROCK1 Protein Expression

To determine whether ROCK1 expression mediates the changes in cardiac fibrosis caused by angiotensin II or pravastatin, we analyzed the cardiac gene and protein expression of ROCK1 (Figs. 4 and 5). With real time-PCR and western blot analysis, the ROCK1 expression was significantly increased by an infusion of angiotensin II. Moreover, this Ang II-induced increase was almost completely abrogated by pravastatin administration. The quantitative analysis of ROCK1 was normalized against the GAPDH expression level.

DISCUSSION

The present study demonstrated that pravastatin can improve diastolic dysfunction and cardiac remodeling as well as hypertrophy and fibrosis in angiotensin II-induced hypertensive mice. These beneficial effects of pravastatin were independent of cholesterol lowering or blood pressure decrease and were associated with statins' pleiotropic effects including improving or restoring endothelial function and decreasing vascular inflammation. These findings suggest the potential involvement of ROCK1.

Fukuta et al[11] have examined the effects of statin therapy in 137 patients with DHF and revealed a significant survival benefit in those who received statin therapy. However, the exact mechanisms of statins possibly explaining the decreased cardiovascular morbidity and mortality in patients with DHF have not been elucidated. Thus, the present study extends the previous observation by demonstrating that statins can inhibit DHF through cholesterol-independent pathway. The pleiotropic effects of pravastatin on LV structure may contribute to the improved diastolic dysfunction. It might not be attributable to

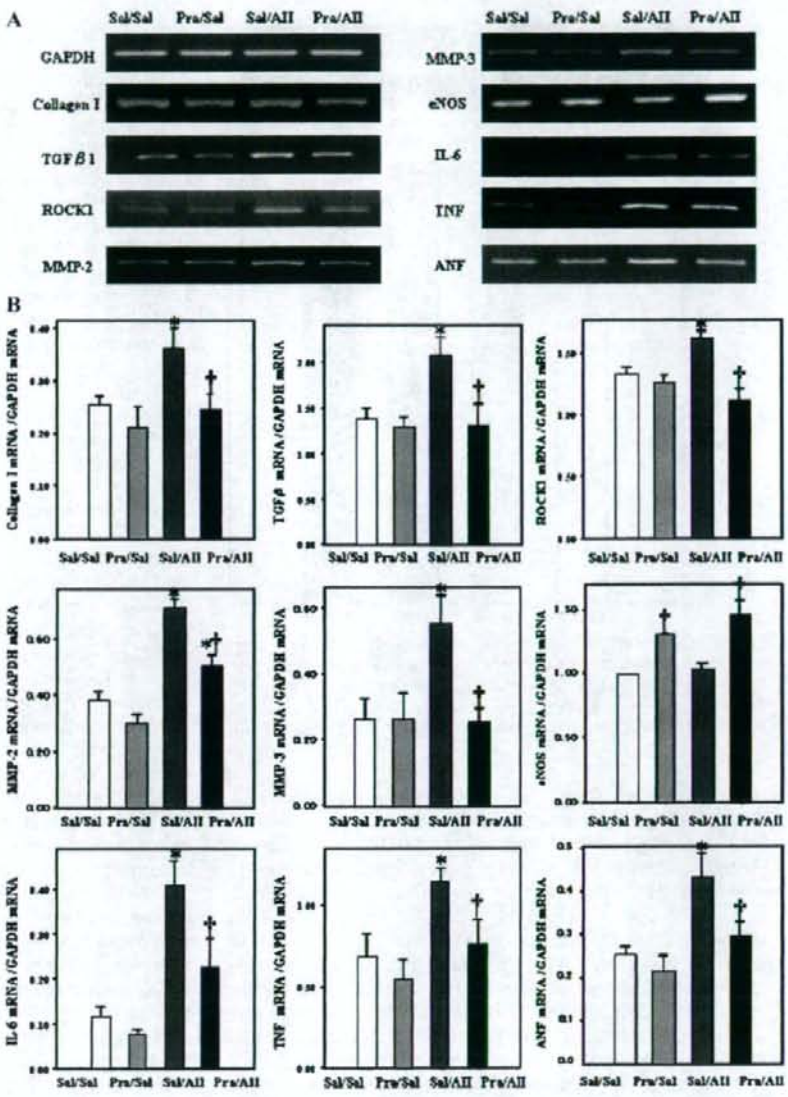

FIGURE 4. A, Expressions of collagen 1, TGF-β, eNOS, MMPs, ANF, IL-6, TNF-α, and ROCK1 mRNA levels in left ventricles of mice were analyzed using RT-PCR and GAPDH as a housekeeping gene. B, The quantitative real-time PCR for collagen 1, TGF-β, eNOS, MMPs, ANF, IL-6, TNF-α, and ROCK1 in left ventricles of mice. The quantitative real-time PCRs were normalized against GAPDH expression. Values are means ± SEM (Sal/Sal: n = 8, Pra/Sal: n = 9, Sal/AII: n = 15, Pra/AII: n = 16). *$P < 0.05$ vs. Sal/Sal and Pra/Sal; †$P < 0.05$ vs. Sal/AII.

its favorable hemodynamic effects because blood pressure and heart rate were not altered.

By inhibiting L-mevalonic acid synthesis, statins also prevent the synthesis of other important isoprenoid intermediates of the cholesterol biosynthetic pathway, such as farnesylpyrophosphate (FPP) and geranylgeranylpyrophosphate (GGPP), which serve as important lipid attachments for the posttranslational modification of a variety of proteins.[12] Because Rho is a major target of geranylgeranylation, inhibition of Rho and its downstream target, Rho kinase, is a likely mechanism mediating some of the pleiotropic effects of statins on cardiovascular disease.[13] Recent studies with the ROCK inhibitors,[14,15] fasudil and Y27632, and with the targeted deletion of ROCK1 mice[4,5] reveal the involvement of ROCK in cardiac hypertrophy and fibrosis. Our study observed that pravastatin treatment significantly attenuated the increase of ROCK1 expression in mRNA and protein level induced by angiotensin II infusion, suggesting the potential involvement of ROCK1 in cardiac remodeling and DHF.

Several possibilities can explain the beneficial effects of pravastatin on myocardial structure and function. Firstly, among the extracellular matrix proteins, collagen I is a major determinant of myocardial stiffness, the amount of which in the heart depends not only on its production but also on its

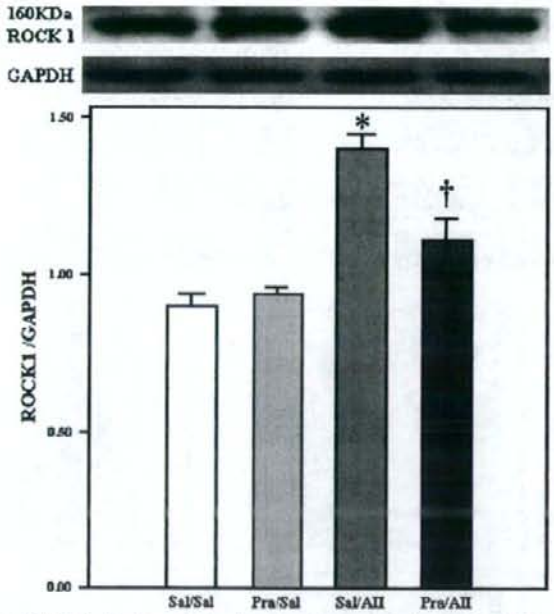

FIGURE 5. Western blots showing the protein level of ROCK1. Bar graph shows result of densitometric analysis of intensity of ROCK1 relative to that of GAPDH protein. Values are means ± SEM (Sal/Sal: n = 8, Pra/Sal: n = 9, Sal/AII: n = 15, Pra/AII: n = 16). *$P < 0.05$ vs. Sal/Sal and Pra/Sal; †$P < 0.05$ vs. Sal/AII.

degradation carried out by matrix metalloproteinases (MMPs). The TGFβ-collagen cascade is thought to be a powerful mediator of myocardial fibrosis.[16-19] Studies have demonstrated that Rho/ROCK signaling plays an important role in the activation of TGFβ and its downstream pathways both in vivo[4,5,20] and in vitro.[21] The activated MMPs have been implied in the development of LV failure[22] and an MMP inhibitor has been shown to limit the chamber dilatation in a murine model of myocardial infarction.[23] Furthermore, in vitro studies have observed that fluvastatin inhibits the production of MMPs.[24] Our data showed that the TGF-β, collagen I, and MMPs mRNA expressions were enhanced in AII-treated mice and that these alterations were significantly attenuated by the treatment with pravastatin. Taken together, one proposed mechanism of pravastatin for reverse remodeling might be related to the attenuation of increased TGF-β, collagen I, and MMPs levels induced by Ang II infusion. In addition, pravastatin might also possess anti-inflammatory properties by their ability to reduce the number of inflammatory cells, which in turn could modulate the expression of proteolytic enzymes, including MMPs. However, the present study does not provide direct proof of a cause-and-effect relation between MMP inhibition and the attenuation of LV failure after pravastatin treatment, and further investigation is needed.

Atherosclerosis is the disorder in the majority of patients with cardiovascular disease.[25] It is also a complex inflammatory process that is characterized by the presence of inflammatory cells. Many cardiovascular studies have suggested that statins have anti-inflammatory effects independent of cholesterol lowering.[26,27] As proinflammatory cytokines, TNF-α and IL-6 were induced by Ang II infusion and pravastatin treatment significantly abolished these increases in the present study. Therefore, anti-inflammatory effects of pravastatin might also be involved in its beneficial effects on LV remodeling.

Finally, the upregulation of eNOS might also contribute to the effects of pravstatin. NO has been shown to inhibit several components of the atherogenic process, such as inhibition of vascular smooth muscle proliferation[28] and endothelium-leukocyte interactions.[29,30] In fact, the salutary effects with statins subjected to hypoxia[31] and oxidized LDL,[32] conditions that lead to endothelial dysfunction, have been attributed to the restored eNOS activity. Therefore, statins might exert many favorable effects on the endothelium and attenuate endothelial dysfunction in the presence of atherosclerotic risk factors. Some recent findings are consistent with a noncholesterol-lowering effect of statins and suggest that inhibition of Rho/ROCK by statins mediates the increase in eNOS expression. Thus Rho/ROCK inversely regulates eNOS expression through alteration in eNOS mRNA stability. Collectively, in our model, the contribution of NO might be an important mechanism by which pravastatin improved endothelial dysfunction, because pravastatin treatment significantly increased eNOS expression compared with Sal/AII-treated mice.

In this study, angiotensin II infusion caused significant increases in total and LDL cholesterol levels, which did not decreased with pravastatin treatment. Hirano et al have also reported that angiotensin II infusion led to significant elevations in TC (total cholesterol) and non-HDL-cholesterol and olmesartan treatment could reverse those changes in fructose-fed rats. It was speculated that the selective activation of AT1R might explain why the plasma cholesterol rises in response to AII infusion.[33] However, the exact mechanism underlying AII-induced hypercholesterolemia is still unknown and further experimental work will be required. Statins have been reported to reduce blood pressure in a randomized, double-blind crossover trial[34] and in hypertensive rodent models,[35,36] whereas angiotensin II did increase blood pressure and pravastatin had no effect on systolic blood pressure in angiotensin II-induced hypertensive mice. This difference may be related to the model, species differences, or the dose of angiotensin II or pravastatin.

Statins' pleiotropic effects on cardiovascular system are dependent in a complex interplay between many factors and processes, and the precise mechanisms responsible for these effects remain to be clearly determined. However, recent study has shown that the cholesterol-independent effects of statins are related to endothelin-1, oxidative stress, MMPs, AT1 receptor, and so on.[37] All of these findings suggest that the inhibition of cardiac remodeling and diastolic dysfunction by statin may be not solely due to only one process or one pathway.

In conclusion, the current study has shown that pravastatin, an HMG-CoA reductase inhibitor, improves diastolic dysfunction and attenuates cardiac remodeling in an angiotensin II-induced hypertensive murine model. These effects include improving or restoring endothelial function and

decreasing vascular inflammation, which are independent of any change in lipid profiles or blood pressure. These findings suggest the potential involvement of ROCK1. Our findings should provide a novel mechanism to explain the pathophysiology of DHF and the clinical benefits of statins in treatment of DHF. While clinical studies are warranted, these initial findings may prove beneficial in shedding some light on the mechanisms of statins for further experimental and randomized clinical trials.

REFERENCES

1. Liao JK, Laufs U. Pleiotropic effects of statins. *Annu Rev Pharmacol Toxicol*. 2005;45:89–118.
2. Liao JK. Effects of statins on 3-hydroxy-3-methylglutaryl coenzyme A reductase inhibition beyond low-density lipoprotein cholesterol. *Am J Cardiol*. 2005;96:24F–33F.
3. Liao JK, Seto M, Noma K. Rho kinase (ROCK) inhibitors. *J Cardiovasc Pharmacol*. 2007;50:17–24.
4. Rikitake Y, Oyama N, Wang CY, et al. Decreased perivascular fibrosis but not cardiac hypertrophy in ROCK1 +/− haploinsufficient mice. *Circulation*. 2005;112:2959–2965.
5. Zhang YMJ, Bo GE, Taffet J, et al. Targeted deletion of ROCK1 protects the heart against pressure overload by inhibiting reactive fibrosis. *FASEB J*. 2006;20:916–925.
6. Lee TM, Lin MS, Chou TF, et al. Effect of pravastatin on development of left ventricular hypertrophy in spontaneously hypertensive rats. *Am J Physiol*. 2005;289:220–227.
7. Bezerra DG, Mandarim-de-Lacerda CA. Beneficial effect of simvastatin and pravstatin treatment on adverse cardiac remodeling and glomeruli loss in spontaneously hypertensive rats. *Clin Sci (Lond)*. 2005;108:349–355.
8. Abe Y, Izumi T, Urabe A, et al. Pravastatin prevents myocardium from ischemia-induced fibrosis by protecting vascular endothelia cells exposed to oxidative stress. *Cardiovasc Drug Ther*. 2006;20:273–280.
9. Onozuka H, Fujii S, Mikami T, et al. In vivo echocardiographic detection of cardiovascular lesions in apolipoprotein E-knockout mice using a novel high-frequency high-speed echocardiography technique. *Circ J*. 2002;66: 272–276.
10. Ishibashi Y, Tsutsui H, Yamamoto S, et al. Role of microtubules in myocyte contractile dysfunction during cardiac hypertrophy in the rat. *Am J Physiol*. 1996;271:H1978–H1987.
11. Fukuta H, Sane DC, Brucks S, et al. Statin therapy may be associated with lower mortality in patients with diastolic heart failure: a preliminary report. *Circulation*. 2005;112:357–363.
12. Takemoto M, Liao JK. Pleiotropic effects of 3-hydroxy-3-methylglutaryl coenzyme A reductase inhibitors. *Arterioscler Thromb Vasc Biol*. 2001; 21:1712–1719.
13. Laufs U, Endres M, Stagliano N, et al. Neuroprotection mediated by changes in the endothelial actin cytoskeleton. *J Clin Invest*. 2000;106:15–24.
14. Higashi M, Shimokawa H, Hattori T, et al. Long-term inhibition of Rho-kinase suppresses angiotensin II-induced cardiovascular hypertrophy in rats in vivo: effect on endothelial NAD(P)H oxidase system. *Circ Res*. 2003;93:767–775.
15. Wang YX, da Cunha V, Martin-McNulty B, et al. Inhibition of Rho-kinase by fasudil attenuated angiotesin II-induced cardiac hypertrophy in apolipoprotein E deficient mice. *Eur J Pharmacol*. 2005;512:215–222.
16. Rosenkranz S. TGF-β1 and angiotensin networking in cardiac remodeling. *Cardiovasc Res*. 2004;63:423–432.
17. Schnee JM, Hsueh WA. Angiotensin II, adhesion, and cardiac fibrosis. *Cardiovasc Res*. 2000;46:264–268.
18. Yamazaki T, Komuro I, Yazaki Y. Role of the renrin-angiotensin system in cardiac hypertrophy. *Am J Cardiol*. 1999;83:H53–H57.
19. Brand T, Schneider MD. The TGF β superfamily in myocardium: ligands, receptors, transduction, and function. *J Mol Cell Cardiol*. 1995;27:5–18.
20. Nishikimi T, Matsuoka H. Molecular mechanisms and therapeutic strategies of chronic renal injury: renoprotective effect of Rho-kinase inhibitoe in hypertensive glomerulosclerosis. *J Pharmacol Sci*. 2006;100: 22–28.
21. Watts KL, Spiteri MA. Connective tissue growth factor expression and induction by transforming growth factor-β is abrogated by simvastatin via a Rho signaling mechanism. *Am J Physiol*. 2004;287:L1323–L1332.
22. Spinale FG, Coker ML, Bond BR, et al. Myocardial matrix degradation and metalloproteinase activation in the failing heart: a potential therapeutic target. *Cardiovasc Res*. 2000;46:225–238.
23. Rohde LE, Ducharme A, Arroyo LH, et al. Matrix metalloproteinase inhibition attenuates early left ventricular enlargement after experimental myocardial infarction in mice. *Circulation*. 1999;99:3063–3070.
24. Ikeda U, Shimpo M, Ohki R, et al. Fluvastatin inhibits matrix metalloproteinase-1 expression in human vascular endothelial cells. *Hypertension*. 2000;36:325–329.
25. Kastelein JJ. The future of best practice. *Atherosclerosis*. 1999;143: S17–S21.
26. Vaughan CJ, Gotto AM Jr, Basson CT. The evolving role of statins in the management of atherosclerosis. *J Am Coll Cardiol*. 2000;35:1–10.
27. Pruefer D, Scalia R, Lefer AM. Simvastatin inhibits leukocyte-endothelial cell interactions and protects against inflammatory processes in normocholesterolemic rats. *Arterioscler Thromb Vasc Biol*. 1999;19:2894–2900.
28. Garg UC, Hassid A. Nitric oxide-generating vasodilators and 8-bromocyclic guanosine monophosphate inhibit mitogenesis and proliferation of cultured rat vascular smooth muscle cells. *J Clin Invest*. 1989; 83:1774–1777.
29. Gauthier TW, Scalia R, Murohara T, et al. Nitric oxide protects against leukocyte-endothelium interactions in the early stages of hypercholesterolemia. *Arterioscler Thromb Vasc Biol*. 1995;15:1652–1659.
30. Kubes P, Suzuki M, Granger DN. Nitric oxide: an endogenous modulator of leukocyte adhesion. *Proc Natl Acad Sci USA*. 1991;88:4651–4655.
31. Laufs U, Fata VL, Liao JK. Inhibition of 3-hydroxy-3-methylglutaryl coenzyme A reductase blocks hypoxia-mediated down-regulation of endothelial nitric oxide synthase. *J Biol Chem*. 1997;272:31725–31729.
32. Laufs U, La Fata V, Plutzky J, et al. Upregulation of endothelial nitric oxide synthase by HMG CoA reductase inhibitors. *Circulation*. 1998;97: 1129–1135.
33. Hirano T, Ran J, Adachi M. Opposing actions of angiotensin II type 1 and 2 receptors on plasma cholesterol levels in rats. *J Hypertens*. 2006;24: 103–108.
34. Glorioso N, Troffa C, Filigheddu F, et al. Effect of the HMG-CoA reductase inhibitors on blood pressure in patients with essential hypertension and primary hypercholesterolemia. *J Hypertens*. 1999;34: 1281–1286.
35. Delbosc S, Cristol JP, Descomps B, et al. Simvastatin prevents angiotensin II-induced cardiac alteration and oxidative stress. *J Hypertens*. 2002;40: 142–147.
36. Jiang J, Roman RJ. Lovastatin prevents development of hypertension in spontaneously hypertensive rats. *J Hypertens*. 1997;30:968–974.
37. Liao JK. Clinical implications for statin pleiotropy. *Curr Opin Lopodol*. 2005;16:624–629.

Automated Three-Dimensional Analysis of Mitral Annular Dynamics in Patients with Myocardial Infarction Using Automated Mitral Annular Tracking Method

Yasuhiko Takemoto M.D., Ph.D., Takeshi Hozumi M.D., Ph.D., F.A.C.C., Kenichi Sugioka M.D., Hiroyuki Watanabe M.D., Yoshiki Matsumura M.D., Ph.D., Minoru Yoshiyama M.D., Ph.D., Kazuhide Takeuchi, M.D., Ph.D., and Junichi Yoshikawa M.D., Ph.D., F.A.C.C.

Department of Internal Medicine and Cardiology, Osaka City University School of Medicine, Osaka, Japan

Background: A newly developed automated mitral annular tracking method (AMAT) has recently become available and enables us to perform automated analysis of mitral annular dynamics. Purpose: To evaluate mitral annular dynamics using AMAT. Methods: AMAT was performed using a Toshiba Aplio SSA-770 ultrasound system in 15 normal healthy volunteers (group N), 16 patients with anterior MI (group A), and 12 inferior MI (group B). The distance between an annular point at end-diastole and at end-systole (distance D) was automatically measured using AMAT at the basal portion of the anterior, lateral, posterior, inferior, and inferoseptal wall. The angle between the mitral annular plane at end-diastole and the direction of movement of each mitral annular point from end-diastole to end-systole (angle A) was also automatically measured at all five mitral annular points. The coefficients of variation (CV) of both distance D and of angle A were calculated as indices of asynchrony of mitral annular dynamics. Results: CV of distance D in group A (22 ± 9% ($P < 0.01$ vs group N)) and group B (22 ± 10% ($P < 0.01$ vs group N)) were both significantly larger than in group N (13 ± 4%). CV of angle A in group A (15 ± 10% ($P < 0.05$ vs group N)) and group B (15 ± 10% ($P < 0.05$ vs group N)) were also significantly larger than that in group N (8 ± 3%). Conclusion: Automated analysis using AMAT showed that mitral annular dynamics of patients with MI were less symmetrical than in normal healthy volunteers. (ECHOCARDIOGRAPHY, Volume 23, September 2006)

three-dimensional, mitral annulus, automated tracking, myocardial infarction, dyssynchrony

Myocardial infarction (MI) is one of the common diseases that causes deformations in mitral valvular spatial geometry and produces asymmetric mitral annular dynamics.[1–4] However, evaluating these changes by meticulous conventional manual measurements of the distorted substructures in patients with MI is cumbersome and time consuming.[5]

Quantitative assessment of the three-dimensional (3D) geometry and dynamics of the mitral valve apparatus during a cardiac cycle have largely been studied in laboratory animals using sonomicrometry, marker angiography, etc.[1,2] Three-dimensional echocardiography has recently been applied in clinical settings to analyze the 3D geometry and dynamics of the mitral valve complex, with meticulous manual measurements of specific substructures of the mitral valve apparatus.[3,4] Various automated endocardial border tracking techniques have been developed to perform precise subjective assessment of left ventricular (LV) function, LV wall motion abnormalities, or dynamics of the mitral annulus.[6,7]

The advanced automated contour tracking (AACT) method has recently become available as an automated endocardial border tracking technique. When compared with the original automated contour tracking (ACT) method, AACT provides more accurate automated LV border detection, even in cases with suboptimal images, and makes more precise automated

Address for correspondence and reprint requests: Takeshi Hozumi, M.D., Department of Internal Medicine and Cardiology, Osaka City University School of Medicine, 1-4-3, Asahi-machi, Abeno-ku, Osaka 545-8585, Japan. Fax: 81-6-6645-3802; E-mail: thozumi@med.osaka-cu.ac.jp

mitral annular tracking (AMAT) feasible.[8,9] We therefore used the AMAT technique to evaluate mitral annular dynamics in patients with MI, and compared them with normal healthy volunteers.

Methods

Study Population

The study enrolled 15 normal healthy volunteers (15 men, mean age 29 ± 4 years), 16 patients with anterior MI (14 men, 2 women, mean age 64 ± 6 years), and 12 patients with inferior MI (11 men, 1 women, mean age 65 ± 13 years). Each patient had documented evidence of a first MI, and underwent coronary angiography which demonstrated a total occlusion of a coronary artery, without significant stenosis in the other coronary arteries. Patients were selected who had wall motion abnormalities only in the territory of a culprit coronary artery, normal mitral valves, sinus rhythm, and no new episodes of ischemic events when echocardiographic examinations were performed. Patients were excluded if they had clinical or echocardiographic evidence of other cardiac diseases, such as pericardial, infiltrative or congenital heart disease, organic valvular disease, cardiac surgery, pacemaker implantation, or atrial fibrillation or flutter. Informed consent was obtained from all patients at enrollment.

The Principles of the AMAT Method

The AMAT method has been developed as a part of the AACT method with the aim of accurate tracking of mitral annulus. The framework of the AACT method consists of three technologies: (1) weighted separability for the edge detection of the endocardial border, (2) contour smoothing using minimization of the elastic energy, and (3) partial shape constraint contour model. The principles of weighed separability and contour smoothing have been described previously.[10–13] The AMAT method is mitral annular tracking algorithm based on the newly developed partial shape constraint contour model which consists of two technique, contour constraint and pattern matching.[8] In contour constraint, the endocardial contour extraction range is restricted by three sample points, which are placed at the both sides of the mitral annulus and at the apex (Fig. 1). The pattern matching technique is utilized for detecting mitral annular locations. In the pattern matching technique, the intensity patterns around both sides of mitral annulus in end-diastolic phase are stored as template images and the geometrical positions that has the most similar intensity patterns to the template images are detected in search areas for each frame using correlation criteria (Fig. 1). These two newly developed techniques allow more accurate tracking of the mitral annulus.

Advantage of the AACT Method over the ACT Method

The original ACT method just consists of two technologies: (1) weighted separability for the edge detection of the endocardial border, (2) contour smoothing using minimization of the elastic energy. It sometimes generates misidentification of the contours of the left ventricle due to, for instance, the chordae tendineae such as Figure 2 because it is not armed with the technology of partial shape constraint contour model. The AACT method consists of three technologies: (1) weighted separability for the edge detection of the endocardial border, (2) contour smoothing using minimization of the elastic energy, (3) partial shape constraint contour model. With the use of the technology of partial shape constraint contour model, the LV endocardial contour extraction range is restricted by three sample points (Fig. 1), which are placed on both sides of the mitral annulus and the apex and this processing improves trace fitting in cases in which the endocardium cannot be clearly visualized.

Analysis of Mitral Annular Dynamics

AMAT was applied to standard apical four- and two-chamber and long-axis views using a broadband phased-array transducer (2–5 MHz) and the Toshiba Aplio SSA-770 ultrasound system (Toshiba Medical Systems Corporation Tochigi-Ken, Tokyo, Japan).

Three sample points were manually identified at both sides of the mitral annulus and the apex in apical two- and four-chamber and long-axis views of an end-diastolic image (Fig. 1) to create a general structural dictionary image of the mitral annulus. The end-diastolic image was synchronized with the R wave of the ECG, and was defined as an initial frame. Second, image pattern matching was executed and the highest correlation coordinates were selected as the detected annular position for each frame following the initial frame (Fig. 1). As a result of these procedures, the mitral annulus

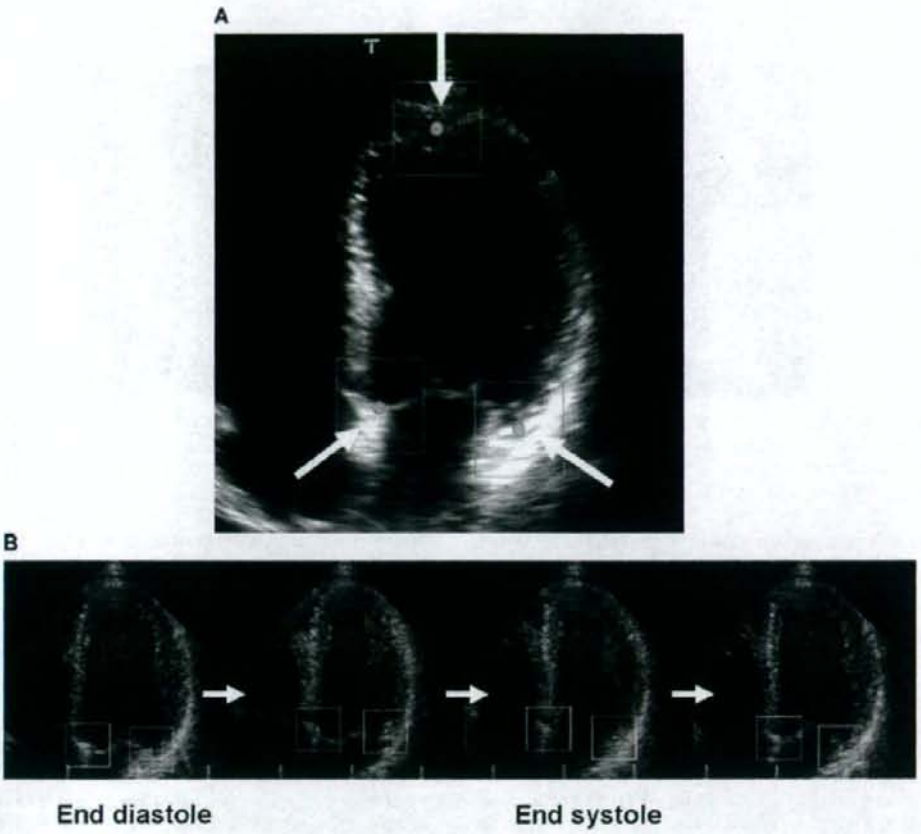

Figure 1. **(A)** *Contour constraint technology. The endocardial contour extraction range is restricted by three sample points, which are placed at both sides of the mitral annulus and the apex. (arrows).* **(B)** *Pattern matching technology. The general structural dictionaries of the mitral annulus are generated and stored. Pattern matching against the stored intensity patterns is performed for each frame in the specified measurement range in order to monitor the position of the mitral annulus.*

was automatically tracked throughout one cardiac cycle using the 2D pattern matching technique. The locations of the mitral annulus were then automatically converted into a graph with the x-axis corresponding to the short axis of the LV, and the y-axis corresponding to the long axis of the LV. The trajectory or motion vector of the mitral annulus was plotted as an X–Y graph.

The distance between an annular point at end-diastole and at end-systole (distance D) was automatically quantified at the basal portion of the anterior, lateral, posterior, inferior, and inferoseptal wall (Fig. 3).

Angle measurements were also performed. Figure 4(A) shows an example of an angle measurement in four-chamber view. As shown in Figure 4(A) left, the mitral annular plane was identified as the line between the two mitral annular points at end-diastole (the green dotted line). The angle (angle A) between the mitral annular plane at end-diastole (the green dotted line) and the direction of movement of each mitral annular point from end-diastole to end-systole (the yellow dotted line) was then automatically measured at both sides of the mitral annulus, as shown in Figure 4(A) right. The same procedures were repeated in two-chamber and long-axis views. When the direction of movement was perpendicular to the mitral annulus plane (see angle β in Fig. 4(A)

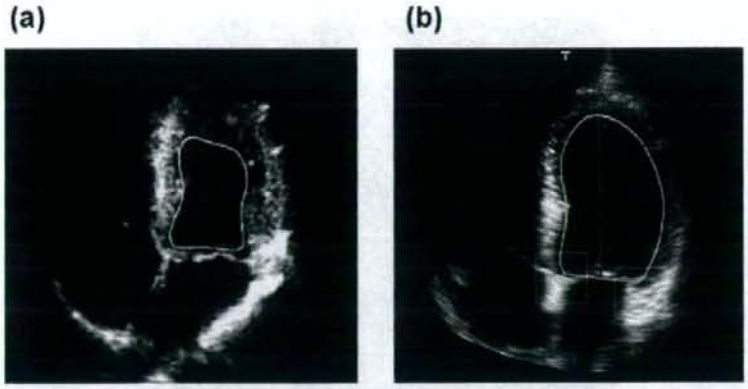

Figure 2. *Advantage of the AACT method over ACT method.* **(a)** *The ACT method sometimes generates misidentification of the contours of the left ventricle due to, for instance, the chordae tendineae because it is not armed with the technology of partial shape constraint contour model.* **(b)** *AACT, with the technology of partial shape constraint contour model, provides improved trace fitting even in cases in which the endocardium cannot be clearly visualized.*

middle), angle A was 90°. When the direction of movement was inward from the perpendicular line (see angle α in Fig. 4(B) left), angle A was less than 90°. When the direction of movement was outward (see angle γ in Fig. 4(B) right), angle A was more than 90°.

Coefficients of variation of distance D and angle A were calculated as indices of asynchrony of mitral annular dynamics. No measurements of the mitral annular point at the subaortic curtain were made, because the structural dictionary of that point differed from that of the other mitral annular points. One investigator performed all measurements, and was blinded to all patient data.

Statistical Analysis

Continuous variables were expressed as mean ± SD. Comparisons of continuous variables between the two groups were made by the unpaired *t*-test. Differences between the groups were assessed by the chi-square test for categorical variables. Distances and angles were compared among the mitral annular points using one-factor ANOVA. Comparisons of coefficient

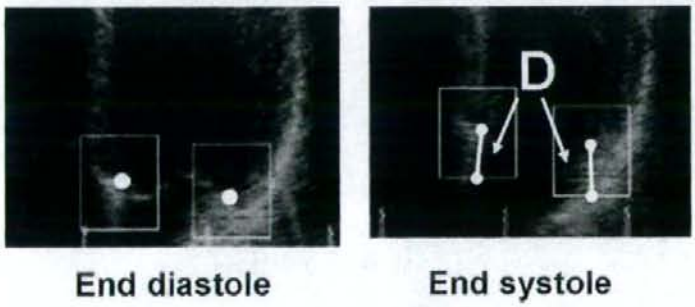

Figure 3. *An example of automated distance measurements in apical four-chamber view of a normal healthy volunteer by AMAT. As the left picture, mitral annular points (white circles) are identified manually at the basal portion of inferoseptal wall and lateral wall in apical four-chamber view at end-diastole. As the right picture, the lower white circles selected as mitral annular points at end-diastole moves to the upper white circles that shows mitral annular points at end-systole. The distances between the lower point and the upper point at each side (distance D) are automatically measured.*

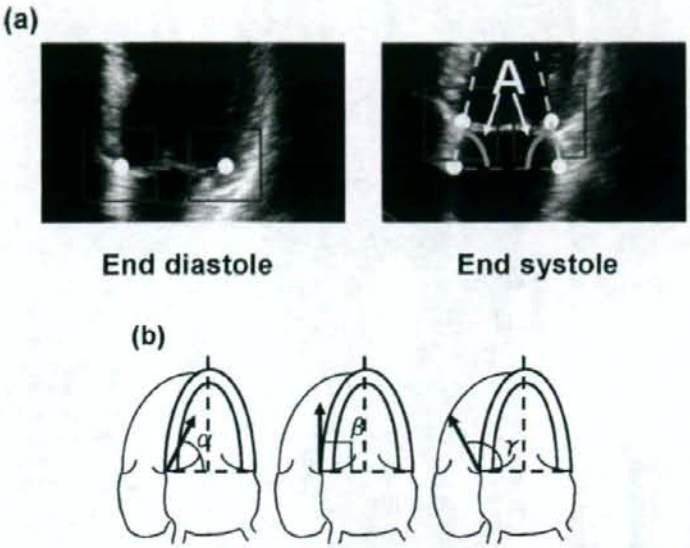

Figure 4. *An example of automated angle measurements in apical four-chamber view of a normal healthy volunteer by AMAT.* **(a)** *As the left picture, mitral annular points (white circles) are identified manually at the basal portion of inferoseptal wall and lateral wall in apical four-chamber view at end-diastole. The line between the two points (the green dotted line) is defined as the mitral annular plane in this view. As the right picture, the lower white circles selected as mitral annular points at end-diastole moves to the upper white circles that show mitral annular points at end-systole so that the moved directions of the mitral annular points are the yellow dotted line. The angles between the green dotted line and the yellow dotted line (angle A) are automatically measured.* **(b)** *When the direction of movement is perpendicular to the mitral annulus plane like β in the middle scheme, angle A is expressed as 90°. When the direction of movement is inward from the perpendicular line like angle α in the left scheme, angle A is shown as less than 90° and outward like angle γ in the right scheme, shown as more than 90°.*

of variation among groups A, B, and N were also made by one-factor ANOVA.

TABLE I

Clinical Characteristics

	Group A n = 16	Group B n = 12	P value
Age (years)	64 ± 8	65 ± 13	0.93
Male gender	14 (88%)	11 (92%)	0.72
Height (cm)	161 ± 9	163 ± 6	0.43
Weight (kg)	62 ± 14	63 ± 7	0.93
SBP (mmHg)	117 ± 16	118 ± 15	0.93
DBP (mmHg)	64 ± 8	65 ± 13	0.72
HR (beats/min)	71 ± 11	73 ± 8	0.75
EDV (ml)	100 ± 27	90 ± 21	0.32
ESV (ml)	57 ± 21	45 ± 14	0.10
EF (%)	45 ± 10	51 ± 8	0.11

SBP = systolic blood pressure; DBP = diastolic blood pressure; HR = heart rate; EDV = end-diastolic volume; ESV = end-systolic volume; EF = ejection fraction.

Results

Sixteen patients with anterior MI (14 men, 2 women, mean age 64 ± 6 years; group A), and 12 with inferior MI (11 men, 1 women, mean age 65 ± 13 years; group B) met the criteria for eligibility in the study. Fifteen normal healthy volunteers were defined as group N.

Clinical Characteristics

Table I presents the baseline clinical characteristics of the 16 patients with anterior MI (group A) and 12 patients with inferior MI (group B). There were no significant differences between group A and group B in both clinical and echocardiographic variables.

Distances and Angles Measured by AMAT

Figure 5(A) shows that distances between one annular point at end-diastole and at end-systole were automatically quantified at the

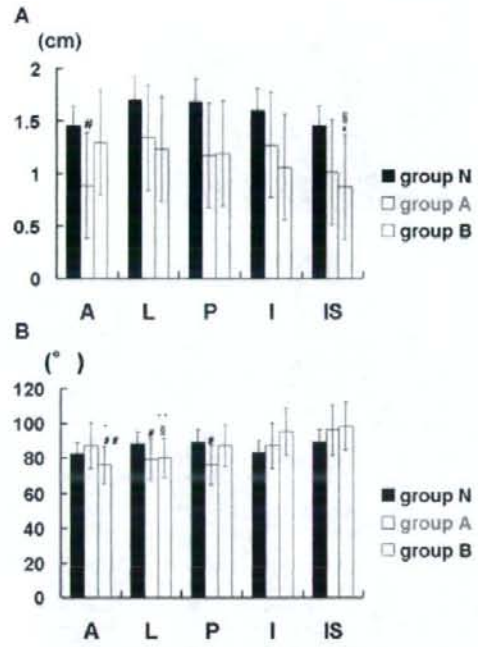

Figure 5. **(A)** *Results of distance measurements. Data are mean distances (cm). A = anterior; L = lateral; P = posterior; I = inferior; IS = inferoseptum.* $^{\#}P < 0.01$ *versus L in group A,* $^{\S}P < 0.01$ *versus L in group B,* $^{*}P < 0.01$ *versus A in group B.* **(B)** *Results of angle measurements. Data are mean angles (°). Abbreviations as in Figure 5(A).* $^{\#}P < 0.01$ *versus IS in group A,* $^{*}P < 0.01$ *versus I in group B,* $^{\#\#}P < 0.01$ *versus IS in group B,* $^{**}P < 0.01$ *versus I in group B,* $^{\S}P < 0.01$ *versus IS in group B.*

basal portion of the anterior, lateral, posterior, inferior, and inferoseptal wall by AMAT. In group N, there were no significant differences between these distances. In group A, distance D at the basal portion of the anterior wall was significantly less than for other basal portions ($P < 0.01$). In group B, distance D at the basal portion of the inferoseptal wall was significantly less than for other basal portions ($P < 0.01$).

Figure 5(B) demonstrates the angles between the mitral annular plane at end-diastole and the direction of movement of each mitral annular point from end-diastole to end-systole that were automatically measured at all the five mitral annular points by AMAT. In group N, there were no significant differences between the angles. In group A, the angles A at the basal portion of the lateral and posterior walls were significantly smaller than those at the basal portion of the inferoseptal wall ($P < 0.01$). In group B, the angles A at the basal portion of the anterior and lateral walls were significantly smaller than those at the basal portion of the inferoseptal wall ($P < 0.01$).

Asynchrony of Mitral Annular Dynamics

Coefficients of variation of distance D and angle A were calculated as indices of asynchrony of mitral annular dynamics. Coefficients of variation of distance D in groups N, A, and B were 13 ± 4, 22 ± 9, and $22 \pm 10\%$, respectively. Coefficients of variation of distance D in group A and in group B were significantly larger than in group N ($P < 0.01$) (Fig. 6A). Coefficients of variation of angle A in groups N, A, and B were 8 ± 3, 15 ± 10, and $14 \pm 6\%$, respectively. Coefficients of variation of angle A in group A and in group B were significantly larger than in group N ($P < 0.05$) (Fig. 6B).

Discussion

The results of this study demonstrate that mitral annular dynamics of patients with MI are less symmetric than in normal healthy volunteers. The newly developed AMAT technique makes automated analyses of mitral annular motion feasible in normal healthy volunteers and in patients with MI.

3D Analysis of Mitral Annulus

Previous studies have demonstrated that regional infarction causes impairment of the mitral annular dynamics in an asymmetric manner.[1,2] They have also shown that infarction modified not only the mitral annulus contiguous to the infracted myocardium, but also the overall mitral annular mechanics. The results of this study are consistent with the previous findings. In this study, patients with anterior MI demonstrated the greatest decrease of distance D at the basal portion of the anterior wall, as well as decreases of distance D at the other four basal portions compared with normal healthy volunteers. The angles A between the mitral annular plane at end-diastole and the direction of movement of all five mitral annular points were also modified. Patients with inferior MI showed the same results. Thus, the overall mitral annular dynamics were asynchronous, in terms of angles as well as distances, compared with normal healthy volunteers.

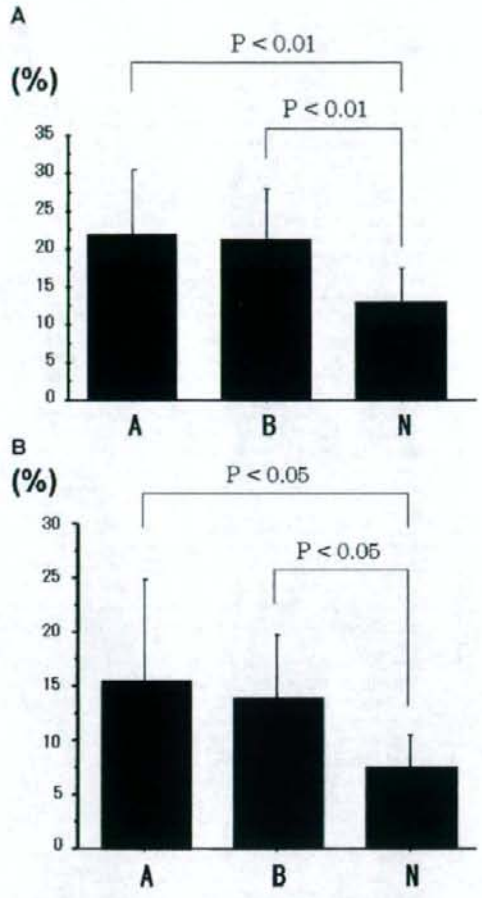

Figure 6. *Comparison of CV* **(A)** *distance measurements. Coefficients of variation of D in groups A, B and N were 22 ± 9, 22 ± 10, and 13 ± 4%, respectively. Coefficients of variation of D in both groups A and B were significantly larger than that in group N (P < 0.01). Data are mean CV (%).* **(B)** *Angle measurements. Coefficients of variation of A in groups A, B, and N were 15 ± 10, 14 ± 6, and 8 ± 3%, respectively. Coefficients of variation of A in both groups A and B were significantly larger than that in group N (P < 0.05). Data are mean CV (%).*

Dynamics of Mitral Annulus Assessed by AMAT

The original ACT method demands very simple manual procedures.[13] However, misidentification of the apex or the mitral annulus in patients with suboptimal images could occur in the old ACT method. The newly developed AACT method adds a new technique to the original ACT method, the partial shape constraint contour model; this consists of two new technologies, pattern matching and contour constraint.[8] It allows precise automated tracking of the mitral annulus, and is named "AMAT" to emphasize the focus of this study. The AMAT method assesses mitral annular dynamics in three planes, and overcomes the shortcomings of the previous ACT method, which only assessed a single plane.

Clinical Implications

The AMAT method depicted mitral annular motions very simply and clearly in patients with MI and in normal healthy volunteers. It demonstrated that MI induced asynchronous mitral annular dynamics compared with normal healthy volunteers. Regarding mechanisms of ischemic mitral regurgitation (MR), some recent reports have shown that increased tethering distance from the medial papillary muscles to the mitral annulus was one of the strongest contributors to ischemic MR.[4,14,15] Other reports have shown that distorted mitral annular dynamics also contributed to ischemic MR.[1,2] The AMAT method may be suitable for investigating the mechanisms of ischemic MR attributable to mitral annular dynamics.

Attention has recently been focused on cardiac resynchronization therapy (CRT) which alleviates LV performance in patients with low ejection fraction and asynchronous LV wall motion abnormalities.[16,17] Although tissue Doppler imaging has been used to evaluate the efficacy of therapy, it is still cumbersome to analyze synchrony of LV wall motion. Velocities measured by tissue Doppler signals depend upon the incident angles of the ultrasound beams, so that analyses by tissue Doppler imaging always require angle corrections. The AMAT method may become an alternative to assess LV synchrony quickly and simply, because it does not require any angle corrections.

Study Limitations

In this study, assessments of mitral annular dynamics were performed on each 2D echocardiographic picture, and the distances and the angles were not recorded simultaneously. Further developments of technique are necessary to make 3D evaluation of the mitral annular mechanics feasible without reconstruction.

In order to evaluate the effects of MI on the mitral annular dynamics as precisely as possible, patients selected for this study had documented evidence of a first MI, and showed hypokinesis or akinesis only in the territory of a culprit coronary artery. However, a wide range of infarct sizes, wall motion abnormalities, and geometric distortions were included in both group A and group B. Further investigations in larger patient groups are necessary to confirm the results of this study.

Conclusions

Automated analyses of mitral annular dynamics using the AMAT method were feasible and showed that mitral annular motions in patients with MI were less synchronous than in normal healthy volunteers. The AMAT method may be a useful tool to evaluate patients with MI.

Acknowledgments: We thank Ryoichi Kanda, MS, Hiroyuki Tsujino, MS, Masahide Nishiura, MS, Naoki Yoneyama, BS, of Toshiba and Toshiba Medical Systems Corporation, for their technical assistance in developing the AMAT method.

References

1. Gorman JH III, Gorman RC, Jackson BM, et al: Distortion of the mitral valve in acute ischemic mitral regurgitation. *Ann Thorac Surg* 1997;64:1026–1031.
2. Glasson JR, Komeda M, Daughters GT II, et al: Three-dimensional dynamics of the canine mitral annulus during ischemic mitral regurgitation. *Ann Thorac Surg* 1996;62:1059–1068.
3. Kwan JK, Shiota T, Agler DA, et al: Geometric differences of the mitral apparatus between ischemic and dilated cardiomyopathy with significant mitral regurgitation. *Circulation* 2003;107:1135–1140.
4. Otsuji Y, Handschumacher MD, Liel-Cohen N, et al: Mechanism of ischemic mitral regurgitation with segmental left ventricular dysfunction: Three-dimensional echocardiographic studies in models of acute and chronic progressive regurgitation. *J Am Coll Cardiol* 2001;37:641–648.
5. Yiu SF, Enriquez-Sarano M, Tribouilloy C, et al: Determinants of the degree of functional mitral regurgitation in patients with systolic left ventricular dysfunction. *Circulation* 2000;102:1400–1406.
6. Perez JE, Waggoner AD, Barzilai B, et al: On-line assessment of ventricular function by automatic boundary detection and ultrasound backscatter imaging. *J Am Coll Cardiol* 1992;19:313–320.
7. Lang RM, Vignon P, Weinert L, et al: Echocardiographic quantification of regional left ventricular wall motion with color kinesis. *Circulation* 1996;93:1877–1885.
8. Nishiura M, Yuasa M, Watanabe M: Active contour extraction method using partial shape constraint contour model. *Syst Comput Jpn* 2000;31:20–28.
9. Sugioka K, Hozumi T, Watanabe H, et al: Rapid and accurate noninvasive assessment of global left ventricular systolic function using biplane advanced automated contour tracking method. *J Am Soc Echocardiogr* 2003;16:1237–1243.
10. Cipolla R, Blake A: The dynamic analysis of apparent contours: *Proc 3rd Int J Comput Vis* 1990;I:616–623.
11. Menet S, Saint-Marc P, Medioni G: Active contour models: Overview, implementation and application. *IEEE Proc Int Conf Syst., Man Cybern.* 1990;6:194–199.
12. Kass M, Witkin A, Terzopoulos D: Snakes: Active contour models. *Int J Comput Vis* 1988;I:321–331.
13. Hozumi T, Yoshida K, Yoshioka H, et al: Echocardiographic estimation of left ventricular cavity area with a newly developed automated contour tracking method. *J Am Soc Echocardiogr* 1997;10:822–829.
14. Otsuji Y, Gilon D, Jiang L, et al: Restricted diastolic opening of the mitral leaflets in patients with left ventricular dysfunction: Evidence for increased valve tethering. *J Am Coll Cardiol* 1998;32:398–404.
15. Otsuji Y, Handschumacher MD, Schwammenthal E, et al: Insights from three-dimensional echocardiography into the mechanism of functional mitral regurgitation: Direct in vivo demonstration of altered leaflet tethering geometry. *Circulation* 1997;96:1999–2008.
16. Sogaard P, Egeblad H, Pederson AK, et al: Sequential versus simultaneous biventricular resynchronization for severe heart failure: Evaluation by tissue Doppler imaging. *Circulation* 2002;106:2078–2084.
17. Sogaard P, Egeblad H, Kim WY, et al: Tissue Doppler imaging predicts improved systolic performance and reversed left ventricular remodeling during long-term cardiac resynchronization therapy. *J Am Coll Cardiol* 2002;40:723–730.

J Pharmacol Sci **101**, 31 – 39 (2006)

Journal of Pharmacological Sciences

Full Paper

Effects of Erythropoietin on Cardiac Remodeling After Myocardial Infarction

Daisuke Nishiya[1,*], Takashi Omura[1], Kenei Shimada[2], Ryo Matsumoto[1], Takanori Kusuyama[1], Soichiro Enomoto[1], Hiroshi Iwao[3], Kazuhide Takeuchi[1], Junichi Yoshikawa[2], and Minoru Yoshiyama[1]

[1]*Department of Internal Medicine and Cardiology, Osaka City University Medical School, 1-4-3 Asahimachi, Abeno-ku, Osaka 545-8585, Japan*
[2]*Department of Medicine Cardiovascular Division, Osaka Ekisaikai Hospital, 2-1-10 Honden, Nishi-ku, Osaka 550-0022, Japan*
[3]*Department of Pharmacology, Osaka City University Medical School, 1-4-3 Asahimachi, Abeno-ku, Osaka 545-8585, Japan*

Received November 30, 2005; Accepted March 2, 2006

Abstract. Erythropoietin (EPO) has been suggested to have a cardioprotective effect against ischemia. The purpose of this study was to examine the effects of EPO on cardiac remodeling after myocardial infarction (MI). MI was induced by ligation of the coronary artery in Wistar rats. The rats with MI were randomly divided into untreated MI and two EPO-treated MI groups. EPO was administered subcutaneously by injection once a day for 4 days after MI at 5000 U/kg or 3 times a week for 4 weeks at 1000 U/kg. Five days after MI, EPO prevented the increase in activated caspase 3, matrix metalloproteinase-2, and transcriptional activation of activator protein-1 in non-infarcted myocardium. Four weeks after MI, left ventricular weight, left ventricular end-diastolic pressure, and left ventricular dimension were increased, and ejection fraction and E wave deceleration time were decreased. EPO significantly attenuated this ventricular remodeling and systolic and diastolic dysfunction. In addition, EPO significantly attenuated the interstitial fibrosis and remodeling-related gene expression in non-infarcted myocardium. Furthermore, EPO significantly enhanced angiogenesis and reduced apoptotic cell death in peri-infarcted myocardium. In conclusion, when administered after MI, EPO prevents cardiac remodeling and improves ventricular function with enhanced angiogenesis and reduced apoptosis.

Keywords: myocardial infarction, cardiac remodeling, erythropoietin, angiogenesis, apoptosis

Introduction

Erythropoietin (EPO) is a glycoprotein hormone secreted from the kidney in response to decreased blood O_2 availability due to hypoxia and anemia (1). Since the primary function of EPO is to promote proliferation, differentiation, and survival of erythroid progenitors in the bone marrow, it increases production of red blood cells. Recombinant human EPO is therefore widely used for the treatment of anemia associated with chronic renal failure.

It has recently been found that EPO receptors are also expressed by certain tissues outside of the hematopoietic system, such as endothelial cells, cardiomyocytes, and neurons (2 – 7). In addition, EPO has been shown to have protective effects against ischemic injury in the brain (8), spinal cord (9), retina (10, 11), kidney (12), and, most recently, even in myocardium (13 – 17). Current findings suggest that the protective effects of EPO in myocardial infarction (MI) depend on the anti-apoptotic effect of this cytokine. Recombinant human EPO reduced apoptosis and final infarct size in rats with MI, and these effects were accompanied by a reduction in decline of left ventricular contractile performance (13 – 15).

Because these cardioprotective effects have for the most part been investigated and observed in the acute phase of MI, the effects of EPO treatment on cardiac

*Corresponding author. ndaisuke@med.osaka-cu.ac.jp
Published online in J-STAGE
DOI: 10.1254/jphs.FP0050966

remodeling after MI are still unclear.

In the present study, we examined the effects of EPO treatment on activated caspase 3, matrix metalloproteinase-2 (MMP-2), and transcriptional activities of activator protein-1 (AP-1) in the subacute phase of MI and infarct size, cardiac remodeling, and systolic and diastolic function four weeks after MI, as well as myocardial fibrosis, apoptosis, angiogenesis, and expression of cardiac remodeling-related genes in non-infarcted myocardium.

Materials and Methods

Animals and experimental design

The investigation conforms with the Guide for the Care and Use of Laboratory Animals published by the US National Institutes of Health (NIH Publication No. 8523, revised 1996).

MI was induced in male Wistar rats weighing 290 – 310 g (Clea Japan, Osaka), as previously described (18). Briefly, the rats were anesthetized by injection of pentobarbital sodium (35 mg/kg, i.p.) and a left thoracotomy was performed under volume-controlled mechanical ventilation (tidal volume, 3.0 ml; respiratory rate, 60 cycles/min). Ligatures were then placed around the left anterior descending coronary arteries. Similar surgery was performed in sham-operated rats but without coronary artery ligation.

The rats with MI were randomly divided into untreated MI and EPO-treated MI groups. EPO was provided by Kirin Brewery Co., Ltd. (Osaka). EPO was administered subcutaneously by injection once a day for 4 days after MI at 5000 U/kg (EPO-H group, n = 8) or 3 times a week for 4 weeks at 1000 U/kg (EPO-L group, n = 8). The rats in the untreated MI group (n = 8) were administered vehicle (0.9% sodium chloride solution) in the same manner.

Western blot analysis

Protein extracts (20 μg) from noninfarcted myocardium at five days after MI were separated on a 12% SDS-polyacrylamide gel and immobilized on polyvinylidene difluoride membrane. The membrane was immunoblotted with anti-phospho-ERK antibodies (Promega, Madison, WI, USA), anti-ERK antibodies (Santa Cruz Biotechnology, Inc., Santa Cruz, CA, USA), anti-phospho-p38 MAPK antibodies (New England Biolabs, Inc., Ipswich, MA, USA), anti-p38 MAPK antibodies (New England Biolabs, Inc.), anti-activated Caspase 3 (Abcam Ltd., Cambridge, UK) and MMP-2 (Daiichi Fine Chemical Co., Ltd., Toyama) using the ECL method for Western blot analysis. An optical scanner (EPSON GT-8000; Seiko, Tokyo) was used for digitization of Western blots to allow for the measurement of phosphorylated proteins or of the total amount of protein. The densities of each band in digitized images of individual gels were measured using the public domain NIH Image program.

Electrophoretic mobility shift assay for AP-1

For the electrophoretic mobility shift assay, nuclear protein extracts at five days after MI were prepared as described previously (19). The sequence of the double-stranded oligonucleotide used in the present study was as follows: consensus AP-1, 5'-CGCTTGATGACTC AGCCGGAA-3'.

Doppler echocardiography and hemodynamic measurements

Four weeks after MI, we performed transthoracic echocardiography on each rat (20). The rats were lightly anesthetized with an injection of ketamine hydrochloride (25 – 50 mg/kg, i.p.) and xylazine (5 – 10 mg/kg, i.p.). Echocardiograms were performed with an echocardiography system equipped with a 7.5-MHz phased-array transducer (SONOS 5500; Philips Medical System, Best, The Netherlands). Two-dimensional short-axis view of the left ventricle and M-mode tracings were recorded through the anterior and posterior left ventricular (LV) walls at the papillary muscle level to measure LV end-diastolic dimension (LVDd) and LV end-systolic dimension (LVDs). LV ejection fraction (EF) was measured by the modified Simpson's method, which used a 4-chamber view. Pulsed-wave Doppler spectra of mitral inflow were recorded from the apical 4-chamber view, with the sample volume placed near the tips of the mitral leaflets in maximal opening with laminar flow pattern.

The method of hemodynamic measurement used was previously described in detail (18). In brief, LV pressure was recorded by inserting a polyethylene-tubing catheter (0.58-mm internal diameter, PE-50) into the right carotid artery and advancing it into the left ventricle. Water-filled catheters were connected to the tubing, which was in turn connected to a water-filled pressure transducer. The pressures were recorded on a physiological recorder, while rats were allowed to breathe spontaneously. LV end-diastolic pressure (LVEDP) was obtained by averaging the values for 10 beats. Myocardial infarct size was measured as previously described (18). Rats with an infarct size of <10% were excluded from analysis. After determination of infarct size, the heart was immediately excised and septal myocardium was dissected as non-infarcted myocardium.

Histological examination

Transverse myocardial sections (5-μm-thick) obtained four weeks after MI were stained with collagen-specific sirius red stain. Each field of non-infarcted myocardium was digitized and the area of interstitial fibrosis was calculated as the ratio of the sum of total area of interstitial fibrosis to the sum of total connective tissue area and cardiomyocyte area in all LV fields of the section. Perivascular areas were not included in this analysis.

TUNEL assay was performed using the ApopTag Apoptosis Detection Kit (Intergen, Burlington, MA, USA) followed by methyl green counterstaining of formalin-fixed, paraffin-embedded sections. Digital photographs were taken under microscopy at ×400 magnification. Twenty-five random high-power fields in the peri-infarct zone of each ventricular sample were chosen and blindly quantified.

Immunohistochemical staining for CD31 (DAKO, Kyoto) and vascular density analysis were performed. After excision, the heart was immediately embedded in OCT compound (Tissue Tek; Miles, Inc., Elkhart, IN, USA), frozen in dry ice/acetone, and cut into 5-μm sections using a cryostat. Five high-power fields in each section were randomly selected in the peri-infarct area, and the number of capillaries in each field was averaged and expressed as the number of capillary vessels per high-power field.

RNA preparation and Northern blot analysis

All procedures were performed as previously described in detail (20). In brief, total RNA was isolated from each heart by the guanidium thiocyanate-phenol-chloroform method. Twenty micrograms total RNA samples were subjected to 1% agarose gel electrophoresis, transferred to nylon membrane, and hybridization was carried out with (^{32}P)-dCTP-labeled cDNA probes for brain natriuretic peptide (BNP), collagen types I and III, osteopontin, plasminogen activator inhibitor-1 (PAI-1), monocyte chemoattractant protein-1 (MCP-1), and rat glyceraldehyde-3-phosphate dehydrogenase (GAPDH). The densities of individual mRNA bands were measured using a bioimaging analyzer (BAS-2000; Fuji Photo Film, Tokyo). For all RNA samples, the density of an individual mRNA band was divided by that of the GAPDH mRNA band to correct for differences in RNA loading and/or transfer.

Statistical analyses

All results are expressed as the mean ± S.E.M. The statistical significance of differences was determined using ANOVA and the Student-Newman-Keuls test. Statistical significance was assumed at $P<0.05$.

Results

Western blot analysis

To analyze the effects of EPO on molecular mechanisms, Western blot analysis was performed from the sample of the non-infarcted myocardium five days after MI. As shown in Fig. 1, EPO did not change the activities of myocardial ERK and p38 MAPK. The activated caspase-3 in the non-infarcted myocardium was significantly increased in the untreated MI group (5.1-fold, $P<0.01$). EPO treatment significantly attenuated the activated caspase-3 compared with the untreated MI group (EPO-L: 66%, $P<0.01$; EPO-H: 60%, $P<0.01$). MMP-2 was significantly increased in the untreated MI group (2-fold, $P<0.01$). EPO significantly attenuated the increase of MMP-2 in the non-infarcted

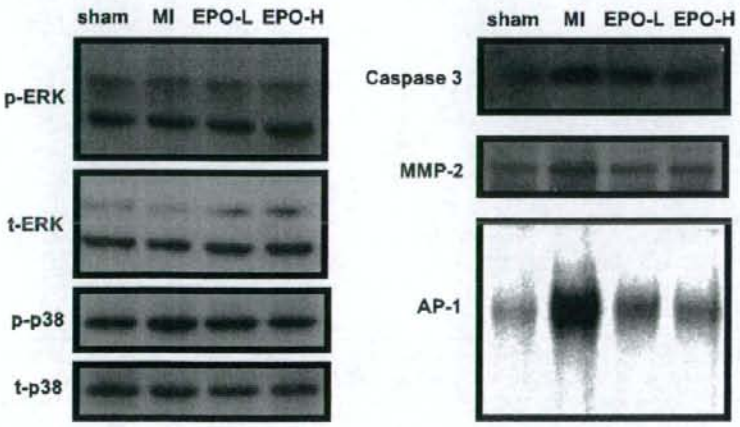

Fig. 1. Effects of EPO on non-infarcted myocardial ERK, p38 MAPK, activated caspase-3, MMP-2, and AP-1 DNA binding activity at five days after MI. The left panels, right top, and right middle panels show representative autoradiographs of Western blot analysis of phosphorylated ERK (p-ERK), total amount of ERK (t-ERK), phosphorylated p38 MAPK (p-p38), total amount of p38 MAPK (t-p38), activated Caspase-3, and MMP-2. The right lower panel shows a representative autoradiograph of gel mobility shift assay of AP-1 DNA binding activity.

myocardium, compared with the untreated MI group (EPO-L: 52%, $P<0.01$; EPO-H: 54%, $P<0.01$).

Electrophoretic mobility shift assay for AP-1

As shown in Fig. 1, MI significantly increased the myocardial transcriptional activity of AP-1 2.5-fold in the non-infarcted myocardium ($P<0.01$). EPO significantly inhibited the increase in the DNA binding activities of AP-1 (EPO-L: 61%, $P<0.01$; EPO-H: 56%, $P<0.01$).

Effects of EPO on ventricular weight, hemodynamics, and infarct size

As shown in Table 1, MI significantly reduced mean blood pressure ($P<0.05$) and increased LVEDP ($P<0.01$) and the LV weight/body weight ratio ($P<0.01$). EPO treatment affected neither heart rate nor mean blood pressure. However, both low and high doses of EPO significantly prevented the increase in weight of the left ventricle (EPO-L, $P<0.05$ and EPO-H, $P<0.01$) and reduced LVEDP (EPO-L, $P<0.01$ and EPO-H, $P<0.05$), compared with rats with untreated MI. Infarct size calculated as fractional area of the scar was significantly smaller in both the EPO-L and EPO-H groups than in the MI group.

Echocardiographic assessment of LV

As shown in Table 1 and Fig. 2, the LVDd and LVDs were significantly higher in the MI group than in the sham-operated group ($P<0.01$ and $P<0.01$, respectively). EPO prevented the increases in both LVDd and LVDs compared with the untreated MI group (EPO-L, $P<0.05$ and $P<0.05$; EPO-H, $P<0.05$ and $P<0.05$, respectively). The MI group exhibited significant systolic dysfunction compared with the sham-operated group, as evidenced by decreased EF ($P<0.01$). Both doses of EPO significantly prevented the decrease in EF (EPO-L, $P<0.01$ and EPO-H, $P<0.05$).

A parameter of diastolic dysfunction, the deceleration time of the E wave was shorter in the untreated MI group than in the sham-operated group ($P<0.01$). EPO significantly prevented worsening of diastolic function after MI in both the EPO-L and EPO-H groups (EPO-L, $P<0.01$ and EPO-H, $P<0.01$). The ratio of E wave to A wave (E/A ratio) in the untreated MI group was significantly increased compared with the sham-operated group ($P<0.05$). In the EPO-L group, E/A ratio was significantly improved compared with the untreated MI group ($P<0.05$). E/A in the EPO-H group did not change compared with the untreated MI group.

Histological and morphometric assessments

As shown in Fig. 3A, sirius red staining revealed a 5.7-fold increase in the fraction of interstitial fibrosis in non-infarcted myocardium in rats with untreated MI compared with sham-operated rats ($P<0.01$). EPO treatment significantly reduced the fraction of interstitial fibrosis (EPO-L: 0.25-fold, $P<0.01$; EPO-H: 0.34-fold, $P<0.01$).

Figure 3B shows enhanced angiogenesis, with a larger

Table 1. Hemodynamics, ventricular weight, and Doppler echocardiographic measurements

	sham	MI		
		untreated	EPO 1000 U/kg	EPO 5000 U/kg
Heart rate (bpm)	319 ± 26	303 ± 31	326 ± 28	319 ± 27
MBP (mmHg)	105 ± 2	93 ± 2*	95 ± 3*	93 ± 5*
LVEDP (mmHg)	9 ± 1	16 ± 2**	10 ± 1††	12 ± 2†
Body weight (g)	355 ± 6	344 ± 4.7	326 ± 4.6**†	330 ± 4.6**
LV/BW (g/kg)	2.09 ± 0.05	2.349 ± 0.03**	2.22 ± 0.049†	2.143 ± 0.042††
RV/BW (g/kg)	0.546 ± 0.007	0.657 ± 0.03	0.621 ± 0.018	0.781 ± 0.08**
MI size (%)	—	38.8 ± 2.3	20.7 ± 5.2†	26 ± 4.4†
LVDd (mm)	7.9 ± 0.2	9.9 ± 0.4**	8.6 ± 0.5†	8.9 ± 0.3†
LVDs (mm)	5.8 ± 0.2	8.6 ± 0.3**	7.0 ± 0.6*†	7.4 ± 0.4*†
EF (%)	59.4 ± 1.1	29 ± 3.6**	45 ± 4.3**††	38 ± 2.7**†
E wave deceleration time (ms)	56.9 ± 1.8	39.1 ± 2.2**	56.6 ± 2.6††	52 ± 1.8††
E/A	1.7 ± 0.2	3.8 ± 0.7*	1.7 ± 0.2†	3.1 ± 0.2*

sham: sham operated rats, MI: myocardial infarction, MBP: mean blood pressure, LVEDP: left ventricular end-diastolic pressure, LV/BW: left ventricle weight/body weight, RV/BW: right ventricle weight/body weight, LVDd: left ventricular dimension end diastole, LVDs: left ventricular dimension end systole, EF: ejection fraction. *$P<0.05$, compared with sham; **$P<0.01$, compared with sham; †$P<0.05$, compared with untreated MI; ††$P<0.01$, compared with untreated MI.

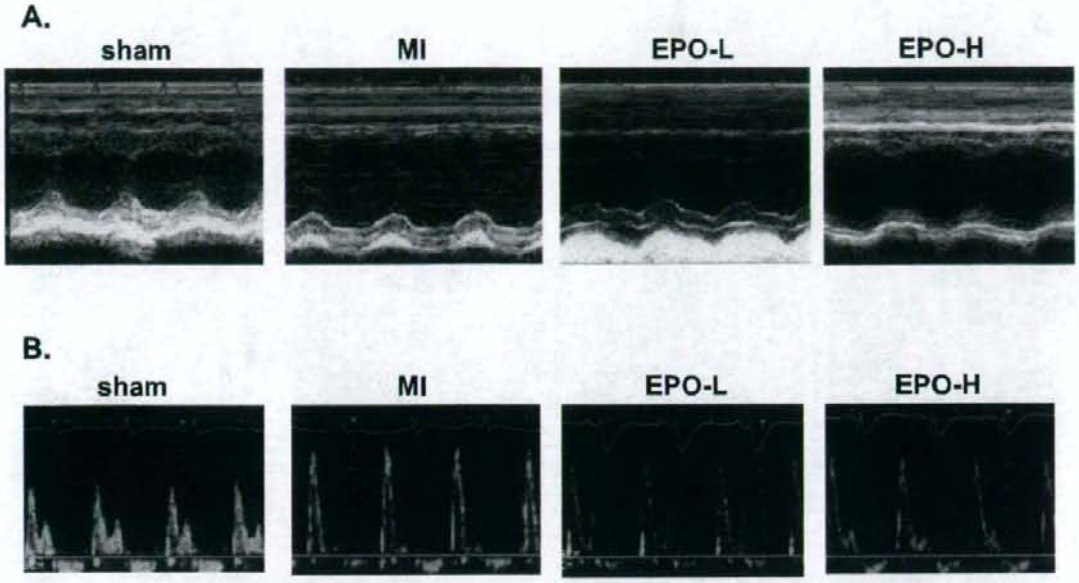

Fig. 2. Echocardiographic assessment 4 weeks after MI. A: LV M-mode echocardiograms (parasternal short-axis view) from a sham-operated rat (sham), a rat with untreated MI (MI), and infarcted rats treated with EPO (EPO-L and EPO-H). B: Examples of pulse-wave Doppler spectra of mitral inflow from a sham-operated rat (sham), a rat with untreated MI (MI), and infarcted rats treated with EPO (EPO-L and EPO-H).

number of capillaries, in the EPO treatment groups (EPO-L: 8.4 ± 0.8 capillaries/HPF, $P<0.01$ to MI; EPO-H: 5.5 ± 0.3 capillaries/HPF, $P<0.05$ to MI; MI: 3.1 ± 0.5 capillaries/HPF). Moreover, EPO-L treatment induced formation of significantly more capillaries than did EPO-H treatment ($P<0.01$).

Figure 3C illustrates TUNEL staining of peri-infarcted myocardium at four weeks after MI. More apoptotic nuclei were observed in untreated MI. Each of the EPO-treated groups exhibited significantly fewer TUNEL-positive nuclei than the untreated MI group (EPO-L: 4.0 ± 0.5 cells/HPF, $P<0.05$ to MI; EPO-H: 5.1 ± 1.1 cells/HPF, $P<0.05$ to MI; MI: 8.5 ± 1.5 cells/HPF).

mRNA expression in non-infarcted myocardium

Figure 4 shows the results of analysis of cardiac gene expression. mRNA expressions of BNP, collagen types I and III, osteopontin, PAI-1, and MCP-1 were significantly increased 4.5-, 4.8-, 3.2-, 5.1-, 3.4-, and 2.2-fold, respectively, at four weeks after MI ($P<0.01$) in non-infarcted myocardium. EPO significantly attenuated the increases in expression of BNP (40%, $P<0.05$), collagen I (58%, $P<0.05$), collagen III (43%, $P<0.05$), osteopontin (43%, $P<0.05$), PAI-1 (38%, $P<0.05$), and MCP-1 (50%, $P<0.05$) mRNA in the EPO-L group. In the EPO-H group, EPO significantly attenuated the increases in expression of BNP (44%, $P<0.05$), collagen I (62%, $P<0.05$), collagen III (63%, $P<0.05$), osteopontin (49%, $P<0.05$), PAI-1 (59%, $P<0.05$), and MCP-1 (45%, $P<0.05$) mRNA.

Discussion

In the present study, we have shown that EPO treatment after MI reduces infarct size, prevents cardiac remodeling, and improves LV function, and also enhances angiogenesis and inhibits myocardial apoptosis. Like short-term treatment with high doses of EPO, long-term treatment with low doses of EPO may thus be an effective strategy for treatment of MI.

We and other investigators have previously reported the preventive effects of angiotensin-converting enzyme (ACE) inhibitor, angiotensin II type 1 receptor blocker (ARB), and other such neurohumoral factor blockers on cardiac remodeling after MI (19 – 21). However, the anti-cardiac remodeling effects of these cardioprotective agents were observed without reduction of infarct size after MI. Notably, though, reduction of infarct size may be one of the main mechanisms by which EPO

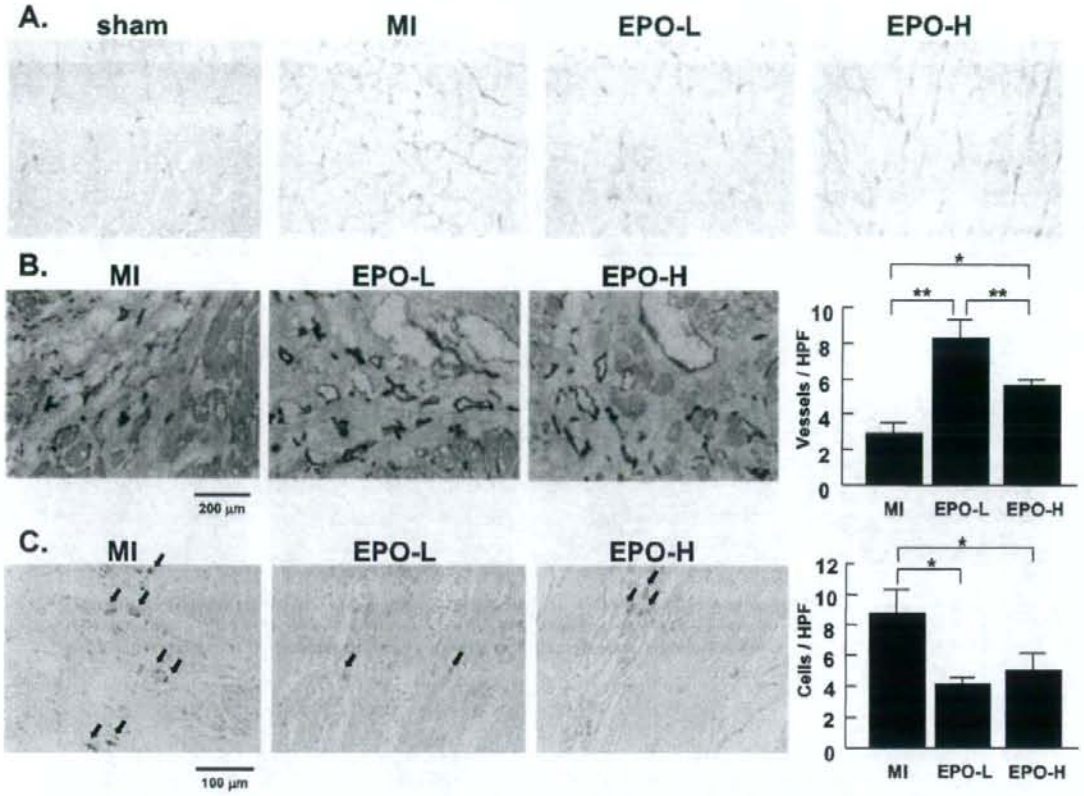

Fig. 3. Histopathological analysis of non-infarcted myocardium of rat left ventricle. A: Photomicrographs show sirius red-stained cardiac sections from sham-operated rats (sham), rats with untreated MI (MI), and infarcted rats treated with EPO (EPO-L and EPO-H). B: Capillary density of peri-infarct region 4 weeks after MI. Sections show immunohistochemical staining for CD31. Capillary density is expressed as the number of capillary vessels per high-power field. Values are each a mean ± S.E.M. *P<0.05, **P<0.01. C: Number of TUNEL-positive cells in the peri-infarct region 4 weeks after MI. Values are each a mean ± S.E.M. *P<0.05.

attenuates cardiac remodeling after MI. It has previously been reported that EPO administered at various time points exerted marked protective effects against ischemia/reperfusion injury and reduced infarct size in rats and rabbits (13 – 17, 22). One of the mechanisms by which EPO may be able to reduce infarct size after MI is anti-apoptotic effects (13 – 15). Also in other organs, EPO exerts protective effects through the inhibition of apoptosis (10 – 12). Activation of Akt and/or PI3 kinase and inhibition of apoptosis are reported to be associated with infarct size-limiting effects of EPO (14). In the present study, activated caspase-3 in the non-infarcted myocardium was reduced in the EPO-treated groups in the subacute phase of MI. Thereafter, the EPO-treated groups exhibited significantly fewer TUNEL-positive nuclei in the peri-infarct area than the untreated MI group. The mean infarct sizes in the EPO-treated MI groups were significantly lower than that in untreated MI. Our findings and those noted in previous reports thus suggest that administration of EPO after MI prevented LV remodeling and reduced infarct size, which may be partially due to inhibition of myocardial apoptosis.

Furthermore, cardiomyocyte apoptosis is not limited to the acute stages of MI but remains increased in the viable myocardium adjacent to infarction even until several weeks after experimental MI (23). Late after MI, apoptosis in the non-infarcted myocardium may play a role in post-MI ventricular remodeling and thus may contribute to the development of congestive heart failure (23). The reduction of apoptosis in the both peri-infarct and non-infarcted myocardium by EPO treatment may

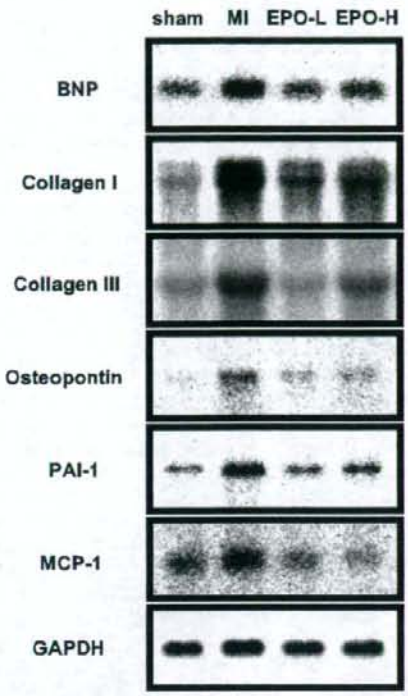

Fig. 4. Effects of EPO on non-infarcted myocardial mRNA expression 4 weeks after MI. Myocardial mRNA expressions of brain natriuretic peptide (BNP), collagen types I and III, osteopontin, plasminogen activator inhibitor 1 (PAI-1), and monocyte chemoattractant protein 1 (MCP-1) were compared in sham-operated rats (sham), rats with untreated MI (MI), and infarcted rats treated with EPO (EPO-L and EPO-H). Each panel shows a representative autoradiogram of Northern blot analysis of BNP, collagen I, collagen III, osteopontin, PAI-1, and MCP-1.

be correlated with the improvement of LV remodeling and the prevention of heart failure.

A significant proportion of the delayed form of myocardial damage occurs as a result of recruitment of inflammatory cells into not only the infarcted region but also non-infarcted regions, in which chemotactic and cytotoxic cytokines and other inflammatory molecules induce cardiomyocyte hypertrophy and myocardial fibrosis and expand the volume of infarct region in an amplifying positive-feedback loop. Previous studies reported anti-inflammatory and cytoprotective effects of EPO (24). In the present study, we measured the DNA binding activity of AP-1 as a key transcriptional factor for cell regulation in a non-infarcted region during cardiac remodeling after MI as we previously reported (19). EPO significantly attenuated the increased activation of non-infarct myocardial AP-1 after MI, thereby suggesting the effects of EPO on transcriptional activation for cardiac remodeling.

Inflammatory cells, which are increased in very early and early stages, produce MMPs that modulate extracellular collagen matrix remodeling. We evaluated the amount of MMP-2 in the non-infarcted myocardium five days after MI. In the EPO-treated groups, MMP-2 was significantly reduced compared with the untreated MI group, thereby suggesting the anti-inflammatory effects of EPO.

In the present study, mRNA expressions of collagen types I and III, osteopontin, PAI-1, and MCP-1 in non-infarcted myocardium were significantly decreased by EPO treatment. We also found that EPO significantly prevented the increase in cardiac fibrosis. Although we did not find significant difference between the expressions of cardiac remodeling-related genes in the EPO-L group and the EPO-H group, the EPO-L group exhibited a trend towards lower expression of these genes. Furthermore, heart failure in the EPO-L group seemed to be more improved with lower expression of BNP than in the EPO-H group. The amount of collagen increased in the non-infarcted myocardium mainly during the late stage after MI, so the EPO treatment during this period may decrease fibrosis and prevent dysfunction much more than short-term EPO treatment.

Another beneficial effect of EPO, enhancement of angiogenesis in the peri-infarct area, may contribute to prevention of cardiac remodeling after MI. It has been shown that EPO induces angiogenesis in a rat aortic ring model (25) and in the chick chorioallantoic membrane (26). It has also been reported that EPO stimulates capillary outgrowth in an in vitro angiogenesis assay using adult human myocardial tissue (27). In the present study, enhancement of angiogenesis with increase in number of capillaries was observed in the EPO treatment groups. The increase of capillary in the peri-infarct area can improve inadequate oxygenation and nutrient supply after MI and prevent apoptosis, reduce progressive collagen deposition and scar formation, and improve ventricular function. Moreover, long-term treatment with EPO induced formation of significantly more capillaries than did short-term treatment. The constant increase of capillary in the peri-infarct area with the long-term EPO treatment can provide adequate oxygenation and nutrient supply and go on preventing progressive cardiac remodeling late after MI. These findings suggest that the neovascularization induced by EPO may play an important role in preventing cardiac remodeling. Long-term treatment with EPO may be particularly effective for enhancement of angiogenesis in the peri-infarct area and can prevent progressive cardiac remodeling late after MI. In the present study, although